# Synthesis of Porous Organic Polymer-Based Solid-Acid Catalysts for 5-Hydroxymethylfurfural Production from Fructose

**Wilhemina Sebati [1,2], Suprakas Sinha Ray [1,2,]\* and Richard Moutloali [2]**

[1]  DST-CSIR National Centre for Nanostructured Materials, Council for Scientific and Industrial Research, Pretoria 0001, South Africa
[2]  Department of Applied Chemistry, University of Johannesburg, Doornfontein, Johannesburg 2028, South Africa
\*  Correspondence: rsuprakas@csir.co.za or ssinharay@uj.ac.za

check for updates

**Abstract:** Herein, we report the synthesis of nanoporous polytriphenylamine polymers (PPTPA) by a simple one-step oxidative polymerization pathway and the materials were sulfonated with chlorosulfonic acid to introduce acidic sulfonic groups to the polymers to form solid acid catalysts (SPPTPA). Magnetic properties were added to SPPTPA catalysts by depositing $Fe_3O_4$ nanoparticles to develop (FeSPPTPA) solid acid catalysts, for performing dehydration of fructose to 5-hydroxymethylfurfural (HMF), which is regarded as a sustainable source for liquid fuels and commodity chemicals. XRD, FTIR spectroscopy, SEM, TGA, and $N_2$ sorption techniques were used to characterize synthesized materials. The FeSPPTPA80 nanocatalyst showed superior catalytic activities in comparison to other catalysts due to the nanorods that formed after sulfonation of the PPTPA polymeric material which gave the catalyst enough catalytic centers for dehydration reaction of fructose. The recyclability tests revealed that the magnetic solid acid catalysts could be reused for four consecutive catalytic runs, which made FeSPPTPA a potential nanocatalyst for production of HMF.

**Keywords:** porous organic polymer; acid catalyst; fructose; dehydration; 5-hydroxymethylfurfural

## 1. Introduction

Researchers are motivated by depleting fossil resources to focus on using renewable biomass feedstock for fuels and value-added chemicals production [1–3]. 5-hydroxymethylfurfural is a lignocellulosic biomass-derived promising platform molecule in various biorefinery systems which is widely used. It is a versatile, attractive molecule and a key intermediate of numerous industrially vital chemicals such as 2,5-Furandicarboxylic acid, 2,5-bis(hydroxymethyl) furan and 2,5-dimethylfuran, which are used for the production of polymers and biofuels [4–7]. In the 19th century, HMF was first separated from a reaction mixture of fructose, sucrose, and oxalic acid, and is currently produced by dehydration of monosaccharides. Solid acid catalysts (such as zeolites, metal oxides, phosphate/phosphonates, sulfuric acid) [8–13] and mineral acids like ($HCl$, $H_2SO_4$, $H_3PO_4$) [14–16] have been reported by many research groups as catalysts for the successful synthesis of HMF. Solid acid catalysts are advantageous above mineral acids since they are non-corrosive, non-toxic, eco-friendly, and diminish other environmental problems related to mineral acids.

Ionic liquids were used as well in the conversion of carbohydrates to 5-HMF [17,18] and to increase the HMF yield, several biphasic systems, i.e., water-methyl isobutyl ketone, water-butanol, and water-THF have also been used [8,14,19–22]. Even though the carbohydrate conversion and selectivity of HMF can be improved by optimizing the reaction conditions, the above liquid acids are still a concern as catalysts because they are not easily separated from reaction mixture causing

issues with product purification and recyclability of the catalyst. Solid acid catalysts can overcome disadvantages of homogeneous catalysts such as organometallic catalysts, as they are capable of modifying the surface acidity and work under harsh reaction environments [21]. The porous organic polymer-based solid acid catalysts possessing high stability and surface area, inexpensive and plentiful active protonic acidic sites on surfaces were used in carbohydrates dehydration [22], but the scope of adding magnetic properties to the catalysts have not been explored. In this work, we report the synthesis of high porous polytriphenylamine (PPTPA) through one-step oxidative polymerization of triphenylamine at temperatures ranging from 80 to 200 °C. The resulted PPTPA polymers were sulfonated by chlorosulfonic acid to the sulfonated polymers (SPPTPA) which were later incorporated with $Fe_3O_4$ nanoparticles to give magnetic polymers (FeSPPTPA). Catalytic results have shown that the catalyst prepared at 80 °C afforded higher catalytic activity in comparison to other catalysts prepared at different temperatures, for the conversion of fructose to HMF with 96.6% yield at 100 °C after the reaction period of 20 min.

## 2. Results and Discussion

### 2.1. Synthesis of FeSPPTPA Solid Acid Nanocatalysts

Scheme 1 shows the preparation of FeSPPTPA nanocatalysts whereby a nanoporous organic polymer (PPTPA) was selected as a precursor for assembly of –$SO_3H$ groups and $Fe_3O_4$ nanoparticles. PPTPA was produced by one-step oxidative polymerization of triphenyl amine in dichloroethane solvent in the presence of $FeCl_3$ catalyst which was later functionalized with chlorosulfonic acid to introduce –$SO_3H$ functional groups to form SPPTPA nanocomposite. The $Fe_3O_4$ nanoparticles were later incorporated in the porous channel as well as the external surface of SPPTPA nanocomposite. This FePPTPA nanocatalyst is insoluble in water and common organic solvents and is thermally stable due to a highly cross-linked structure.
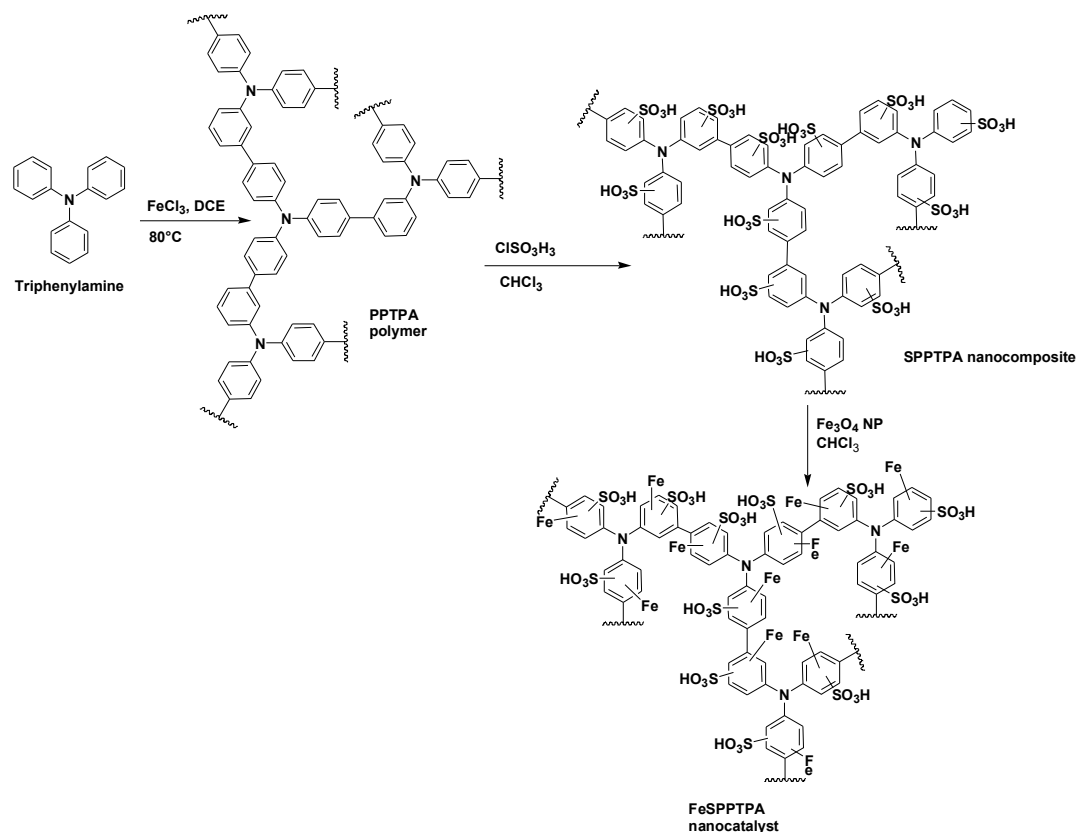


**Scheme 1.** Synthesis of FePPTPA nanocatalysts.

## 2.2. Porosity and Nanostructure

Table 1 and Figure 1 show BET surface areas and $N_2$ adsorption/desorption isotherms of PPTPA, SPPTPA, and FeSPPTPA polymers synthesized at different temperatures. The surface areas and pore volumes of the PPTPA polymers decreased upon sulfonation and incorporation of $Fe_3O_4$ nanoparticles which suggest successful functionalization of aromatic rings with sulfonic acid functional groups, and also indicate successful incorporation of nanoparticles into polymer networks responsible for hindering the $N_2$ adsorption inside the porous channels of PPTPA polymers. PPTPA polymers showed type II isotherms, and their adsorption isotherms show high $N_2$ uptake at very low relative pressure signifying that the materials are microporous. At high $P/P_0$ of $N_2$ desorption, profiles show a wide hysteresis loop confirming the existence of mesopores and swelling of the polymeric network upon gas adsorption resulting from high interaction of polymer-solvent than polymer-polymer interaction. In contrast, adsorption/desorption isotherms of SPPTPA and FeSPPTPA materials showed type I isotherm corresponding to the presence of micropores in this sulfonated nanoparticle incorporated polymers. The resultant pore size distribution of the materials reveal a hierarchical pore structure with two different types of pores and the pore width was also decreased in sulfonated polymers.

Figure 2 shows XRD diffraction patterns of PPTPA, SPPTPA, and FeSPPTPA polymers, where PPTPA patterns displayed broad peaks which could be accredited to amorphous framework structures containing polymerized triphenylamine units randomly distributed. The diffractions may be matched with carbon planes diffractions (002) and (101) [22]. The peaks can also be attributed to the development of regular-ordered pore structure due to monomer units' polymerization through homocoupling. After sulfonation, the intensity of the broad peaks from neat polymers has decreased in some sulfonated polymers which may suggest lowering of the ordered nanostructure. After incorporation of $Fe_3O_4$ nanoparticles to sulfonated polymers, additional sharp peaks were observed indicating that the nanoparticles are well crystallized inside the nanoporous polymer frameworks.

**Table 1.** BET results for polytriphenylamine (PPTPA) polymers.

| Sample | Surface Area ($m^2/g$) | Pore Volume ($cm^3/g$) |
|---|---|---|
| PPTPA80 | 1024 | 0.69 |
| SPPTPA80 | 535 | 0.34 |
| $Fe_3O_4$/SPPTPA80 | 223 | 0.18 |
| PPTPA100 | 994 | 0.66 |
| SPPTPA100 | 506 | 0.32 |
| $Fe_3O_4$/SPPTPA100 | 242 | 0.22 |
| PPTPA120 | 921 | 0.59 |
| SPPTPA120 | 541 | 0.33 |
| $Fe_3O_4$/SPPTPA120 | 246 | 0.21 |
| PPTPA140 | 1156 | 0.79 |
| SPPTPA140 | 644 | 0.42 |
| $Fe_3O_4$/SPPTPA140 | 304 | 0.31 |
| PPTPA160 | 1078 | 0.76 |
| SPPTPA160 | 658 | 0.45 |
| $Fe_3O_4$/SPPTPA160 | 243 | 0.29 |
| PPTPA180 | 873 | 0.64 |
| SPPTPA180 | 444 | 0.33 |
| $Fe_3O_4$/SPPTPA180 | 237 | 0.29 |
| PPTPA200 | 718 | 0.51 |
| SPPTPA200 | 429 | 0.30 |
| $Fe_3O_4$/SPPTPA200 | 207 | 0.26 |

PPTPA: Catalysts prepared at different temperatures. SPPTPA: Sulfonated PPTPA catalysts. $Fe_3O_4$/SPPTPA: Fe nanoparticle incorporated onto SPPTPA.
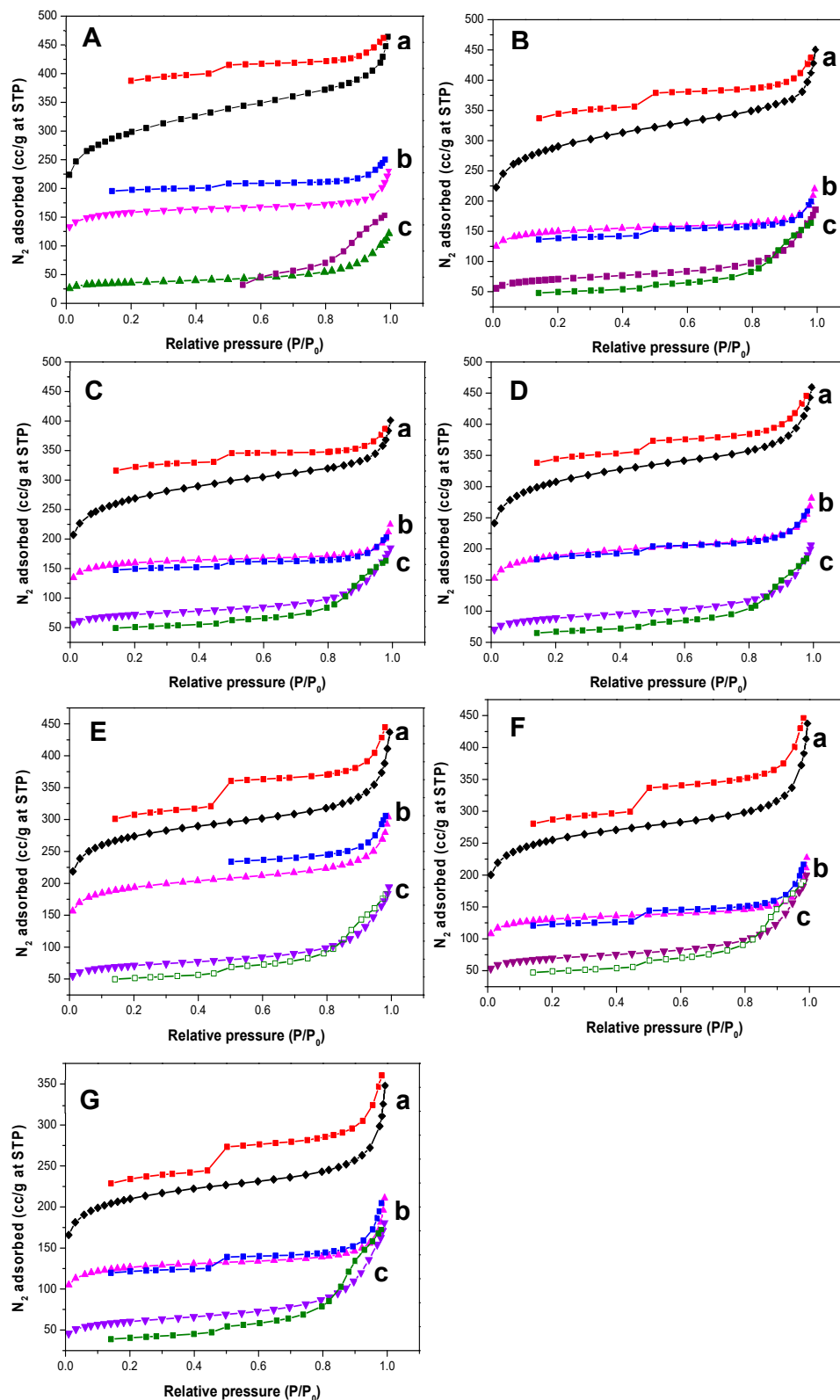
**Figure 1.** N$_2$ adsorption/desorption isotherms of (**a**) neat, (**b**) sulfonated, and (**c**) nanoparticle incorporated PPTPA at (**A**) 80, (**B**) 100, (**C**) 120, (**D**) 140, (**E**) 160, (**F**) 180, and (**G**) 200 °C.
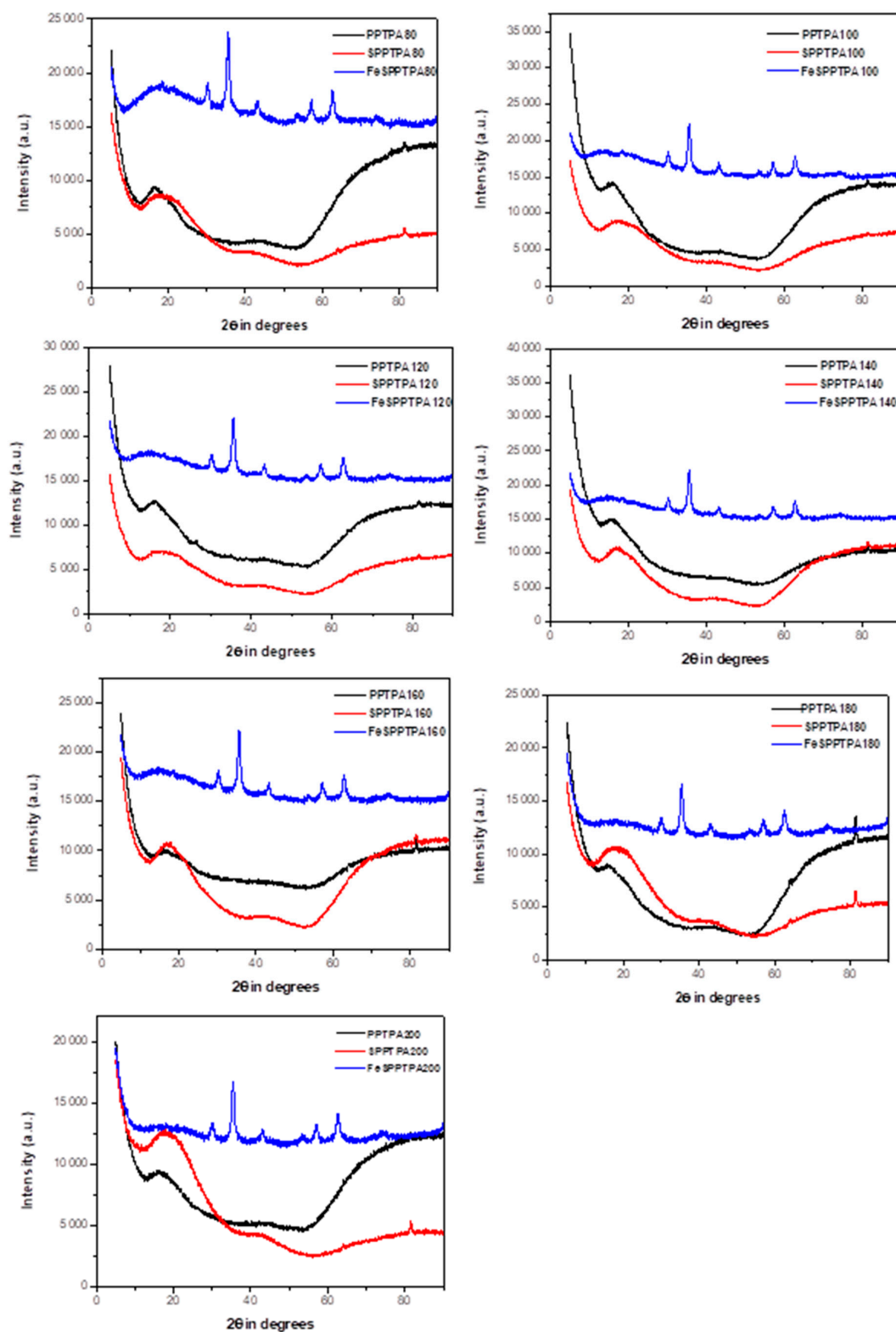
**Figure 2.** XRD patterns of neat, sulfonated and magnetic PPTPA polymers synthesized at different temperature of 80, 100, 120, 140, 160, 180, and 200 °C.

## 2.3. Spectroscopic Results

Figure 3 shows FTIR spectra of neat, sulfonated, and nanoparticle incorporated polymeric materials where the peaks at around 1274 cm$^{-1}$ could be assigned to C-N stretching of the tertiary amines and the peaks at around 815 cm$^{-1}$ could be assigned to C-H out of plane bending of the para-substituted

benzene rings. These suggest a successful coupling of triphenylamine monomers. The spectra of SPPTPA and FeSPPTPA polymers showed extra bands along with all peaks of neat PPTPA polymers signifying the presence of main polytriphenylamine structure in the sulfonated and nanoparticle incorporated materials. The peaks at 1005 and 1031 cm$^{-1}$ may be attributed to the asymmetric O=S=O stretching vibrations, and the peaks at around 3500 cm$^{-1}$ could be assigned to OH group from the –SO$_3$H groups [23].
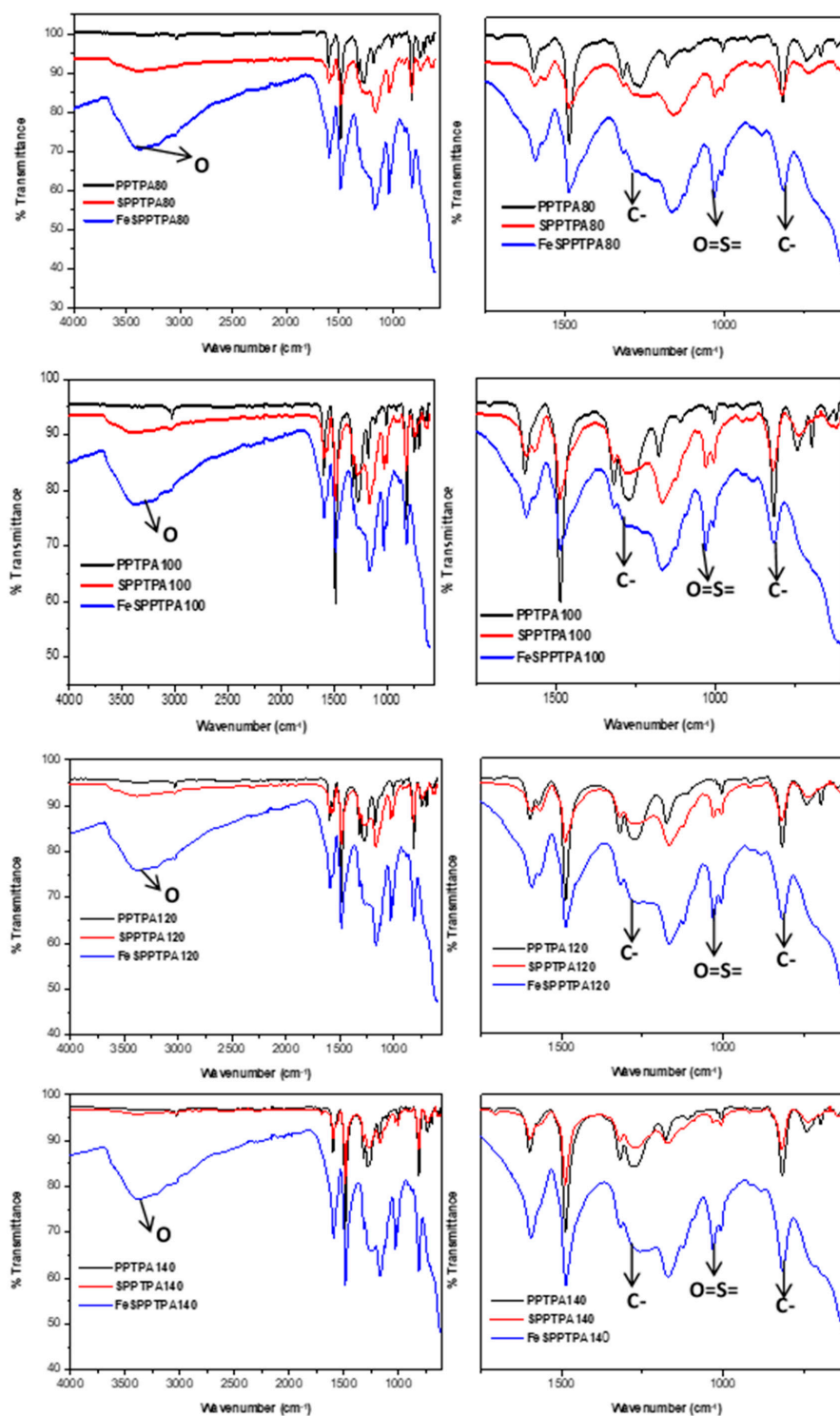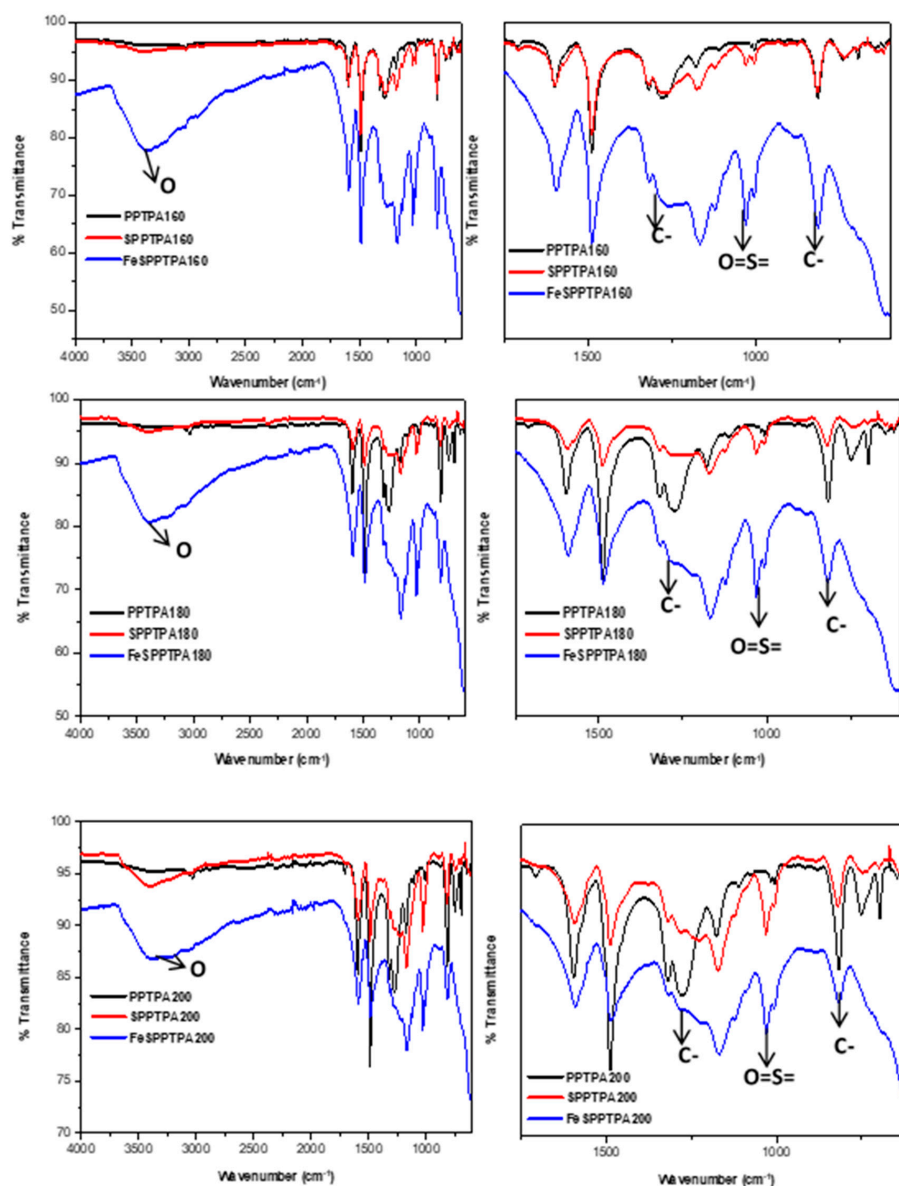


**Figure 3.** *Cont.*

**Figure 3.** FTIR spectra of neat, sulfonated and nanoparticle incorporated PPTPA synthesized at different temperature of 80, 100, 120, 140, 160, 180, and 200 °C.

## 2.4. Electron Microscopic Analysis

Morphologies of the polymeric materials were investigated by SEM analysis, and the images are shown in Figures 4–10. The images revealed that the materials synthesized at 80 °C showed nanofiber-like morphology with infinite length and folding with other nearest fibers. Increasing synthesis temperature changed the morphology from nanofibers to flake-like particles in neat PPTPA, and for sulfonated and nanoparticle incorporated polymers, there was a rod shape for polymers synthesized at low temperatures and the combination of rods and flake-like particles for high-temperature polymers. The formation of nanorods was due to electrophilic para substitution followed by oxidative polymerization with head-to-tail coupling taking place in the presence of $FeCl_3$ and self-polymerization of monomer triphenylamine molecules. At low temperatures, the polymer growth continued in the direction of 001 planes leading to the formation of nanofiber morphology, and at higher temperatures, there was a secondary overgrowth which led to the formation of agglomerated particles. Percentage sulfur loading in sulfonated polymers and iron loading in

nanoparticle incorporated polymers are given in Tables 2 and 3, which does not show any trend in the increase in synthetic temperature.

**Table 2.** Sulfur percentage in sulfonated POPs.

| Sample | % Sulfur |
|--------|----------|
| SPPTPA80 | 5.7 |
| SPPTPA100 | 6.9 |
| SPPTPA120 | 5.5 |
| SPPTPA140 | 3.9 |
| SPPTPA160 | 4.3 |
| SPPTPA180 | 3.8 |
| SPPTPA200 | 4.7 |

**Table 3.** Sulfur and Iron percentage in Magnetic POPs.

| Sample | % S | % Fe |
|--------|-----|------|
| $Fe_3O_4$/SPPTPA80 | 5.7 | 0.9 |
| $Fe_3O_4$/SPPTPA100 | 6.9 | 1.1 |
| $Fe_3O_4$/SPPTPA120 | 5.5 | 1.0 |
| $Fe_3O_4$/SPPTPA140 | 3.9 | 0.6 |
| $Fe_3O_4$/SPPTPA160 | 4.3 | 0.6 |
| $Fe_3O_4$/SPPTPA180 | 3.8 | 0.5 |
| $Fe_3O_4$/SPPTPA200 | 4.7 | 0.3 |
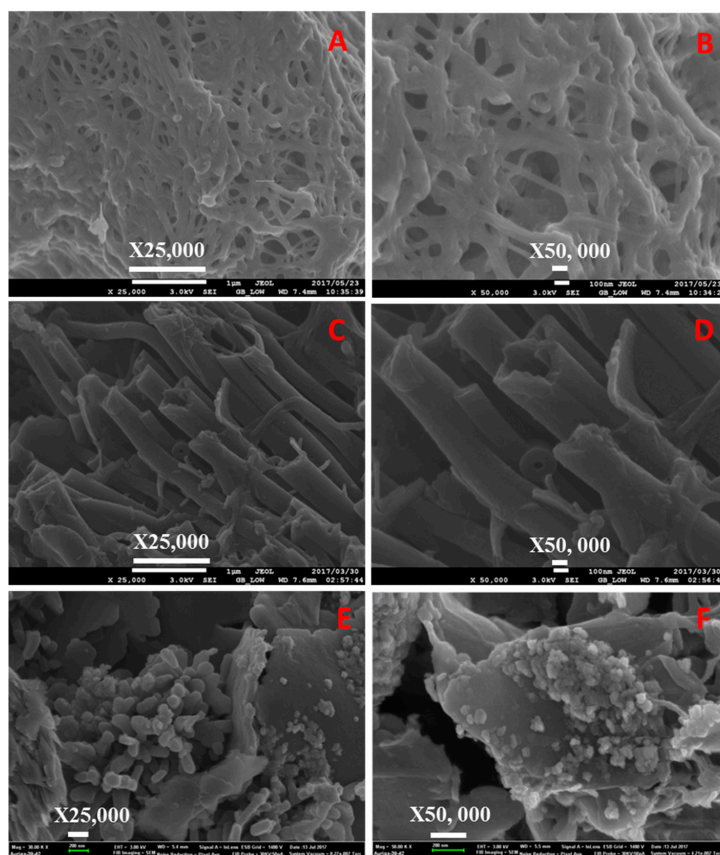


**Figure 4.** SEM images of (**A**,**B**) neat, (**C**,**D**) sulfonated PPTPA, and (**E**,**F**) Fe incorporated SPPTPA at 80 °C.
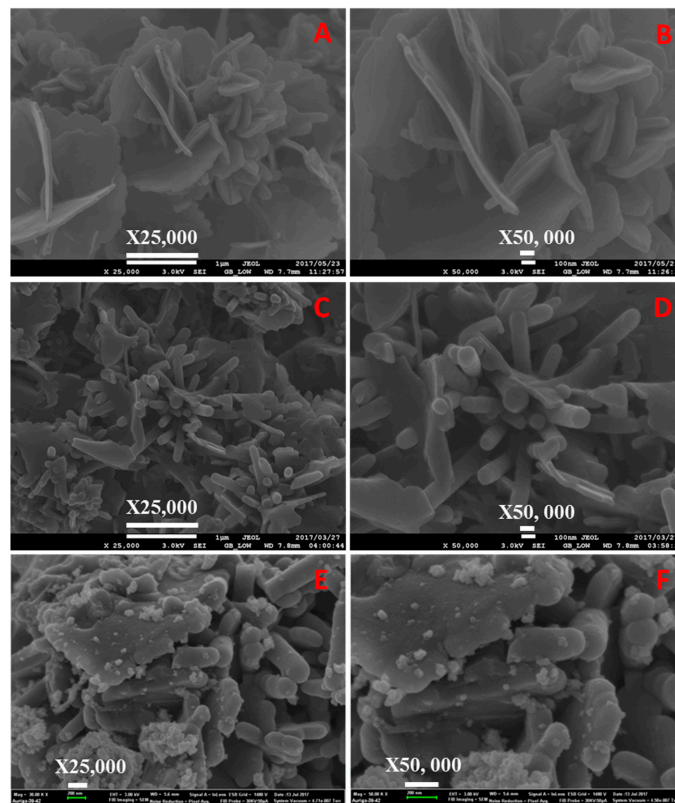
**Figure 5.** SEM images of (**A**,**B**) neat, (**C**,**D**) sulfonated PPTPA, and (**E**,**F**) Fe incorporated SPPTPA at 100 °C.
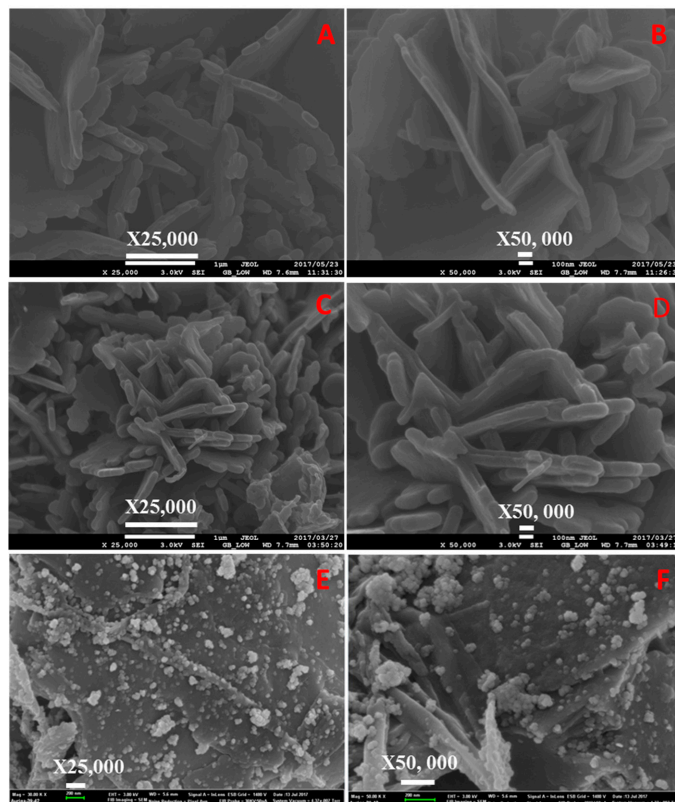


**Figure 6.** SEM images of (**A**,**B**) neat, (**C**,**D**) sulfonated PPTPA, and (**E**,**F**) Fe incorporated SPPTPA at 120 °C.
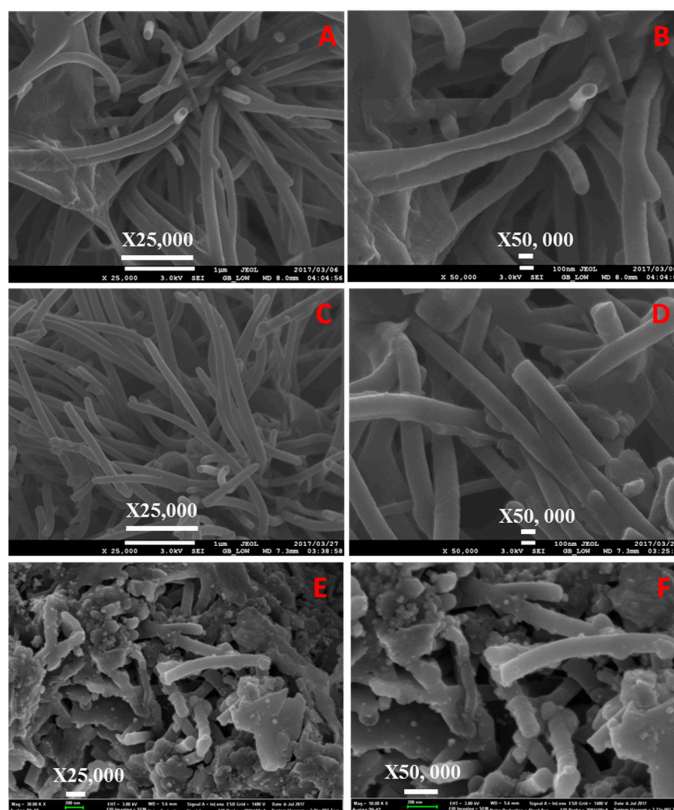
**Figure 7.** SEM images of (**A**,**B**) neat, (**C**,**D**) sulfonated PPTPA, and (**E**,**F**) Fe incorporated SPPTPA at 140 °C.
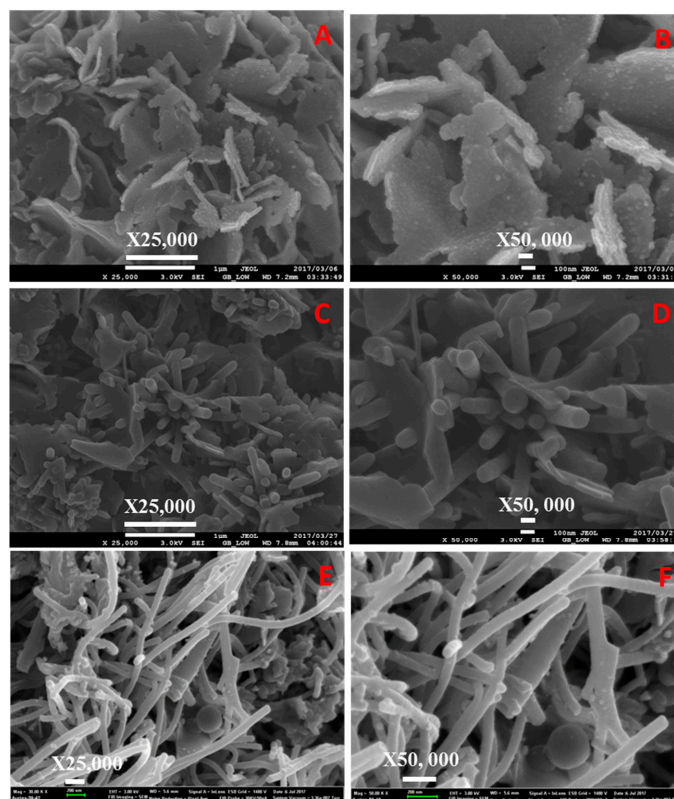


**Figure 8.** SEM images of (**A**,**B**) neat, (**C**,**D**) sulfonated PPTPA, and (**E**,**F**) Fe incorporated SPPTPA at 160 °C.
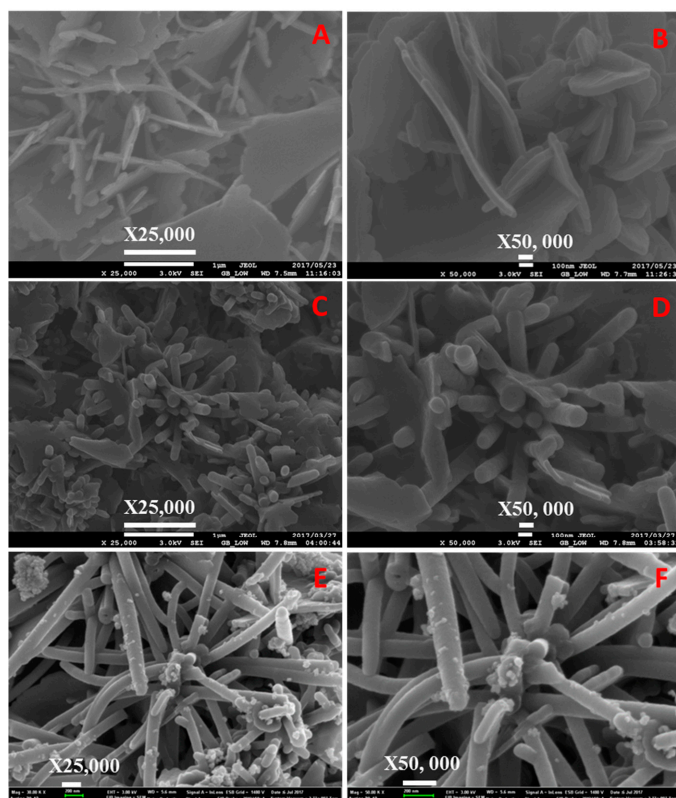
**Figure 9.** SEM images of (**A**,**B**) neat, (**C**,**D**) sulfonated PPTPA, and (**E**,**F**) Fe incorporated SPPTPA at 180 °C.
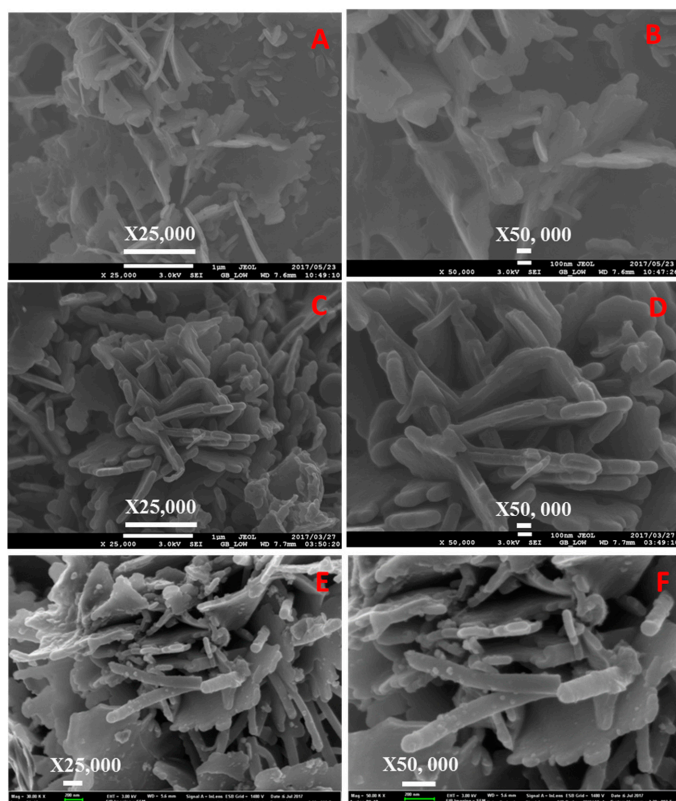


**Figure 10.** SEM images of (**A**,**B**) neat, (**C**,**D**) sulfonated PPTPA, and (**E**,**F**) Fe incorporated SPPTPA at 200 °C.

## 2.5. Thermal Analysis

In Figure 11, the TGA plots of PPTPA, SPPTPA, and FeSPPTPA polymers are shown, whereby PPTPA polymers show the first percentage weight loss in the temperature range 45–55 °C that could be assigned to water molecules intercalated and adsorbed by the materials. The PPTPA polymer materials are thermally stable in a nitrogen atmosphere in the temperature range 500–550 °C. After that temperature range, the thermal cleavage of the PPTPA frameworks starts. The sulfonated and nanoparticle incorporated materials show first weight loss due to the loss of physically adsorbed water molecules in pores followed by strongly adsorbed water molecules having noncovalent interaction with free sulfonic acid groups [23]. Additional weight loss in the temperature range 210–270 °C could be assigned to the loss of free sulfonic acid groups and cleavage of the organic framework takes place beyond 500 °C. High thermal stability of these polymeric materials could be due to the high hyperbranched cross-linking and the rigid polymeric networks in the molecular skeleton.
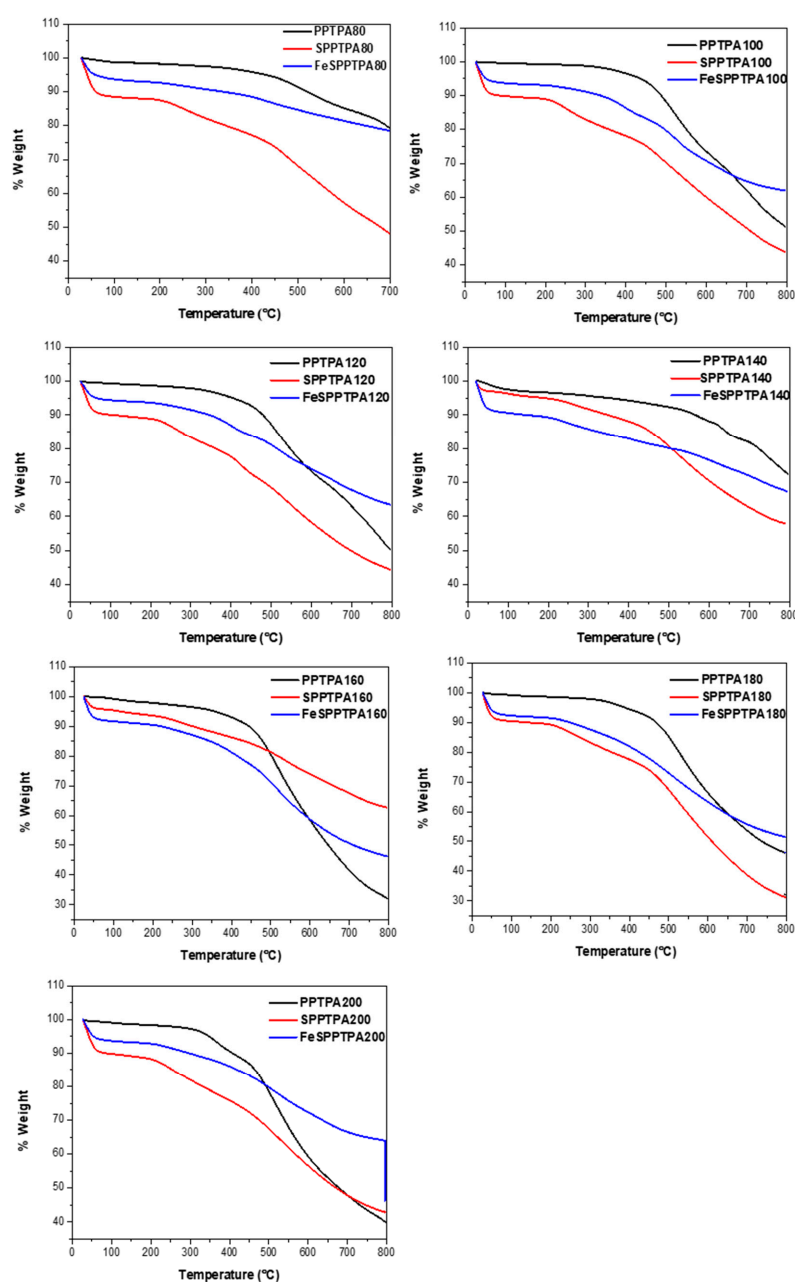


**Figure 11.** TGA plots of neat, sulfonated PPTPA and Fe incorporated SPPTPA polymers synthesized at different temperature of 80, 100, 120, 140, 160, 180, and 200 °C.

### 2.6. Catalytic Dehydration of Fructose to HMF Over FeSPPTPA Catalysts

Catalytic performance of solid acid catalyst has been studied for the conversion of fructose to HMF under different reaction conditions. Fructose (25 mg) and FeSPPTPA catalyst (5 mg) were mixed DMSO solvent (3 mL) under the microwave, room temperature, and reflux conditions at different temperatures from 25 to 120 °C for 20 min and the results are summarized in Table 4. Catalytic conversions could be observed and the HMF yield was 11.7% at 80 °C for FeSPPTPA80 (Table 4, entry 1), and increasing temperature to 100 °C increased HMF yield to 96.6% (Table 4, entry 2). Increasing temperature further from 100 °C to 120 °C, dropped HMF yield from 96.6% to 31.3%. Higher temperature decrease HMF yield because HMF was reported to be unstable under high temperatures [2]. Results in Table 4 (entries 1–25), shows that FeSPPTPA80 was a better catalyst when compared to others as it gave the highest HMF yield of 96.6%. It performed better because the sulfonic groups and Fe nanoparticles were incorporated on a high surface area fibrous polymer material that broke to nanorods after functionalization which gave the catalyst enough catalytic centers for dehydration to take place. The catalytic activity of neat polymer without sulfonic groups showed HMF yield of 9.0% (Table 4, entry 26) which suggested that –$SO_3H$ groups are the primary catalytically active site responsible for the catalytic reaction. Mondal et. al. [24] also reported the synthesis of HMF from biomass using sulfonated polymer and achieved HMF yield of 94.6% at 120 °C for 20 min. Even though the reported catalyst achieved a higher HMF yield, it required a longer time (three days) to be prepared, which makes it difficult and expensive to prepare and the catalyst did not have magnetic properties.

**Table 4.** Conversion of fructose to HMF catalyzed by FeSPPTPA nanocatalysts.

| Entry | Catalyst | Temperature [°C] | Fructose Conversion [%] | HMF Yield [%] |
|---|---|---|---|---|
| 1 | FeSPPTPA80 | 80 | 80.5 | 11.7 |
| 2 | FeSPPTPA80 | 100 | 95.0 | 96.6 |
| 3 | FeSPPTPA80 | 120 | 95.0 | 31.2 |
| 4 | FeSPPTPA100 | 80 | 82.0 | 13.6 |
| 5 | FeSPPTPA100 | 100 | 95.0 | 19.5 |
| 6 | FeSPPTPA100 | 120 | 95.0 | 25.1 |
| 7 | FeSPPTPA120 | 80 | 83.4 | 10.6 |
| 8 | FeSPPTPA120 | 100 | 95.0 | 66.1 |
| 9 | FeSPPTPA120 | 120 | 95.0 | 48.1 |
| 10 | FeSPPTPA140 | 80 | 87.4 | 16.0 |
| 11 | FeSPPTPA140 | 100 | 95.0 | 22.3 |
| 12 | FeSPPTPA140 | 120 | 95.0 | 67.8 |
| 13 | FeSPPTPA160 | 80 | 86.0 | 0.2 |
| 14 | FeSPPTPA160 | 100 | 95.0 | 7.5 |
| 15 | FeSPPTPA160 | 120 | 95.0 | 57.2 |
| 16 | FeSPPTPA180 | 80 | 84.8 | 64.1 |
| 17 | FeSPPTPA180 | 100 | 95.0 | 43.8 |
| 18 | FeSPPTPA180 | 120 | 95.0 | 71.8 |
| 19 | FeSPPTPA200 | 80 | 83.5 | 69.5 |
| 20 | FeSPPTPA200 | 100 | 95.0 | 71.8 |
| 21 | FeSPPTPA200 | 120 | 95.0 | 81.1 |
| 22 | FeSPPTPA80 | 25, microwave | 44.0 | 1.1 |
| 23 | FeSPPTPA80 | 25, room temp | 46.2 | 1.8 |
| 24 | FeSPPTPA80 | 100, room temp | 46.8 | 1.9 |
| 25 | FeSPPTPA80 | 100, reflux | 80.0 | 1.4 |
| 26 | PPTPA | 100 | 95.0 | 9.0 |

Reaction conditions: 5 mg catalyst loading using DMSO (5 mL) as a solvent for 20 min.

### 2.6.1. Solvent Effect

Solvents play a significant role in catalytic reactions under liquid phase, and Table 5 shows results obtained for dehydration of fructose to HMF using different solvents. Amongst the solvents tested, DMSO was identified as the best for the conversion of fructose to HMF, showing high catalytic activity. This was because DMSO has a good microwave absorbing ability [24]. Williams et al. [25] proposed that DMSO performed as a catalyst in dehydration of fructose and Vlachos et al. [26] suggested that

DMSO solvent assemble itself firmly to hydrogen atoms of the hydroxyl groups in fructose, preventing reversion and polymerization products from fructose. Furthermore, DMSO molecules around the C1 atom of HMF hinder HMF rehydration and formation of by-products.

**Table 5.** Influence of solvent in the conversion of fructose to HMF.

| Entry | Solvent | Fructose Conversion [%] | HMF Yield [%] |
|-------|---------|-------------------------|---------------|
| 1 | DMSO | 95.0 | 96.6 |
| 2 | Ethanol | 94.8 | 1.2 |
| 3 | Methanol | 95.0 | 2.2 |
| 4 | THF | 95.4 | 50.1 |
| 5 | Ethylene glycol | 94.8 | 2.8 |

Microwave-assisted heating conditions: 5 mg (FeSPPTPA80) catalyst loading at 100 °C for 20 min using 5 mL solvent.

### 2.6.2. Reaction Time Effect

Investigation of reaction time was done, and the results are presented in Table 6. The HMF yield was 63.5% at 100 °C after 10 min (Table 6, entry 1) and the yield increased to 96.6% after 20 min (Table 6, entry 2). Increasing time from 20 to 30 and 60 min decreased HMF yield from 96.6% to 42.6% (Table 6, entry 3) and 34.3% (Table 6, entry 4). This decrease in HMF yield proposes that the longer the reaction period, the more byproducts from the condensation of HMF [27].

**Table 6.** Dehydration of fructose at different time intervals.

| Entry | Time [min] | Fructose Conversion [%] | HMF Yield [%] |
|-------|-----------|-------------------------|---------------|
| 1 | 10 | 95.0 | 63.5 |
| 2 | 20 | 95.0 | 96.6 |
| 3 | 30 | 95.0 | 42.6 |
| 4 | 60 | 95.0 | 34.3 |

Microwave-assisted heating conditions: 5 mg (FeSPPTPA80) catalyst loading at 100 °C using 5 mL (DMSO) solvent.

### 2.6.3. Catalyst Concentration Effect

Different catalyst concentrations were used to conduct experiments in DMSO solvent (3 mL) for 20 min at 100 °C using FeSPPTPA80 as a catalyst, and the results are represented in Table 7. The results indicated HMF yield of 3.2% was formed when the reaction was conducted in the absence of a catalyst (Table 7, entry 1), suggesting that DMSO acted as both solvent and catalyst in the process of fructose dehydration [25]. The HMF yield of 4.5% was obtained when 2 mg of the catalyst was used (Table 7, entry 2), and the HMF yield increased to 96.6% when 5 mg of the catalyst was used (Table 7, entry 3), followed by a decrease to 14.0% when the catalyst loading was increased to 10 mg (Table 7, entry 4). The results signify that the more the catalyst, the more the acidic sites in the reaction environment which causes HMF product to be further converted to levulinic acid [28].

**Table 7.** Influence of catalyst loading on dehydration of fructose.

| Entry | Catalyst Amount [g] | Fructose Conversion [%] | HMF Yield [%] |
|-------|---------------------|-------------------------|---------------|
| 1 | 0 | 57.0 | 3.2 |
| 2 | 2 | 95.0 | 4.5 |
| 3 | 5 | 95.0 | 96.6 |
| 4 | 10 | 95.0 | 14.0 |

Microwave-assisted heating conditions: 5 mL (DMSO) solvent at 100 °C for 20 min using FeSPPTPA80 catalyst.

### 2.6.4. Catalyst Reusability

Figure 12 shows that the FeSPPTPA80 nanocatalyst could be effectively recycled and reused in up to four consecutive catalytic cycles. At the 4th catalytic cycle, the HMF yield was decreased by 9% compared to the 1st catalytic cycle. This may be due to partial blocking of accessible catalytic active sites (–$SO_3H$ group) inside the porous organic polymer. During the hot filtration test for fructose dehydration to HMF, a 96.3% HMF was observed after 10 min, and the HMF yield did not show any improvement after 20 min when only the filtrate was further run. These results verified that there was no leaching of –$SO_3H$ groups from the nanocatalysts during the reaction indicating the –$SO_3H$ groups are strongly attached to the polymer network. The results also demonstrate that the FeSPPTPA80 catalyst is heterogeneous.
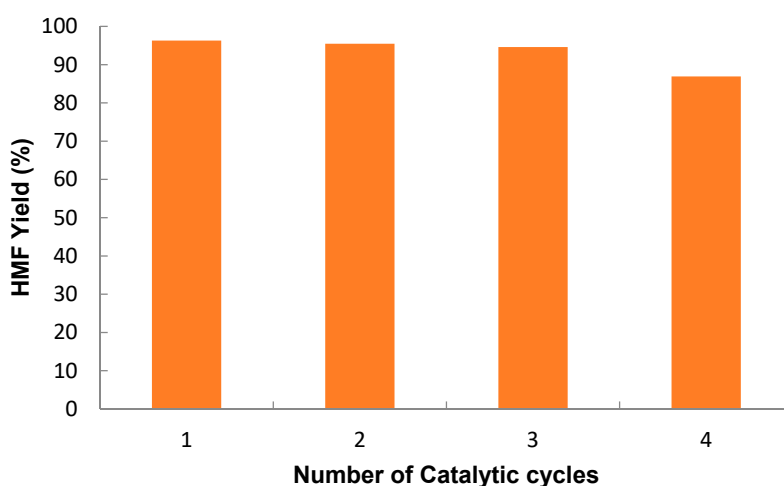
**Figure 12.** Recyclability and reusability of FeSPPTPA80 nanocatalyst. Reaction conditions: fructose (25 mg), FeSPPTPA80 catalyst (5 mg), Temp. 100 °C, microwave irradiation and DMSO solvent (3 mL).

### 2.6.5. Characterization of the Reused Catalyst

The $N_2$ sorption and SEM analysis were used to characterize the reused FeSPPTPA80 catalyst to investigate any visible changes in the catalyst after the 4th catalytic cycle. A BET surface area of 3 $m^2/g$ was revealed, and the substantial decreases in the surface area of the reused catalyst in comparison with the fresh FeSPPTPA80 suggest blockage of the nanoporous channel, which hinders nitrogen from being adsorbed into FeSPPTPA80 catalyst. Figure 13 shows SEM images of the reused FeSPPTPA80 catalyst after the 4th catalytic run which signifies that the catalyst morphology was not changed, implying that the catalyst is thermally and mechanically stable during the catalytic reaction conditions.
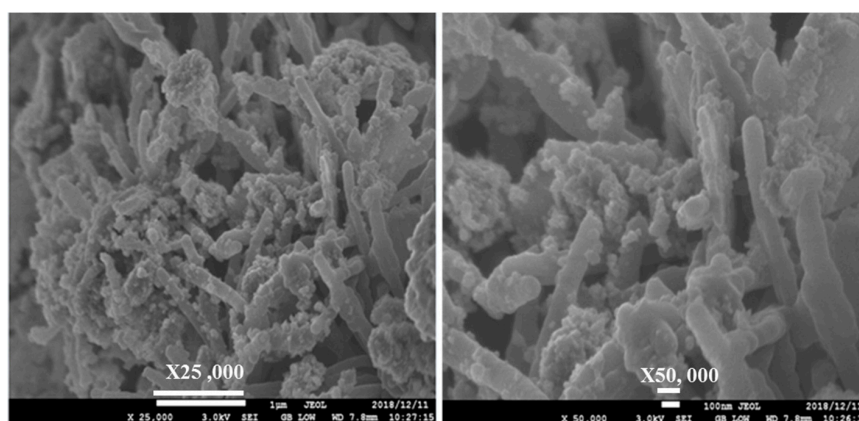
**Figure 13.** FESEM images of reused SPPTPA80 catalyst.

## 3. Experimental

### 3.1. Materials

A 98% reagent grade triphenylamine, 97% reagent grade iron(III) chloride (FeCl$_3$), 97% ACS reagent Iron(III) chloride hexahydrate, 98% reagent grade iron(II) chloride tetrahydrate, and ACS reagent 28–30% NH$_3$ basis ammonium hydroxide solution (NH$_4$OH) were purchased from Sigma-Aldrich, South Africa. Dichloromethane (DCM), 1,2-dichloroethane (DCE), acetone (C$_3$H$_6$O), tetrahydrofuran (THF), methanol (MeOH), and dimethyl sulfoxide (DMSO) were purchased from MINEMA chemicals, Johannesburg, South Africa. The solvents were used as received without further purification.

### 3.2. Synthesis of Neat Porous Organic Polymer PPTPA

Triphenyl amine (491 mg) and anhydrous FeCl$_3$ (973 mg) were dissolved in 1,2-dichloroethane (40 mL) in a microwave vial, and the mixture was stirred for 2 h under hydrothermal microwave at different temperatures (80, 100, 120, 140, 160, 180, and 200 °C). The precipitate was added to acetone (50 mL), and the mixture was filtered, washed with acetone, THF and methanol. The final product was dried at 70 °C for 24 h to yield a blue powder of PPTPA, modified from the method of Mondal et al. [24].

### 3.3. Sulfonation of Porous Organic Polymer

PPTPA polymer (300 mg) was mixed with DCM (30 mL) in a round-bottomed flask and stirred for 2 h. The solution was placed in an ice bath and added chlorosulfonic acid (3 mL) to the mixture over 20 min continuously stirring, and the mixture was further stirred for 24 h at 25 °C. The product was poured into ice, filtered, and washed with distilled water, and dried at 70 °C for 24 h to yield SPPTPA, modified from the method of Modal et al. [24].

### 3.4. Synthesis of Fe$_3$O$_4$ Nanoparticles

Fe$_3$O$_4$ nanoparticles were synthesized from a chemical co-precipitation method in a 2:1 ratio of Fe$^{3+}$ and Fe$^{2+}$ ions. FeCl$_3$·6H$_2$O (5 g) and FeCl$_2$·4H$_2$O (2.5 g) were dissolved in distilled water (100 mL) in a round-bottomed flask. The mixture was purged with nitrogen gas for 30 min, and the aqueous ammonia solution was added dropwise with vigorous stirring until the pH kept constant in the range of 8–9. The reaction mixture was stirred at 60 °C for 30 min. The resulting product was filtered and washed with deionized water and ethanol, and dried at 60 °C for 24 h, modified from the method of Ma et al. [29].

### 3.5. Incorporation of Fe$_3$O$_4$ Nanoparticles in SPPTPA Porous Organic Polymers

SPPTPA polymer (100 mg) was dispersed in DCM (50 mL) by stirring at 25 °C for 2 h. Then Fe$_3$O$_4$ nanoparticles (100 mg) was dissolved in DCM (10 mL) and added to the previous polymer reaction mixture. The resulting reaction mixture was dispersed under sonication for 2 h, and the product was separated by centrifuge, washed with DCM and ethanol, and dried at 60 °C for 24 h.

### 3.6. Dehydration of Fructose to HMF

Dehydration of fructose to HMF was performed in a microwave tube loaded with the desired amount of fructose, catalyst, and solvent (3 mL). The tube was placed in an assisted microwave, and the reaction was performed for 20 min at the preferred temperature. Then the reaction mixture was allowed to cool, then the catalyst was removed from the reaction by magnetic separation technique. The filtrate was analyzed by UV/Vis spectrophotometry. Initially, a standard HMF solution of 99% purity was used for calibration, and after a good correction, the reaction products were analyzed by UV/Vis spectrophotometer.

### 3.7. Reusability of the Catalysts

In a typical recycling experiment of dehydration with FeSPPTPA80 catalyst, a mixture of fructose (25 mg), FeSPPTPA80 nanocatalyst (5 mg), and DMSO (3 mL) in microwave vessel was heated to 100 °C using the hydrothermal assisted microwave for 20 min. The catalyst was separated from the reaction mixture using a magnetic bar, washed with methanol and acetone, dried at 50 °C for 16 h, and used directly for the next catalytic reaction without further purification. The products were analyzed with UV-Vis spectrophotometer.

### 3.8. Hot Filtration Test

Hot filtration test was performed to evaluate the heterogeneous nature of FeSPPTPA80 nanocatalyst. In this typical experiment, fructose (25 mg), FeSPPTPA80 (5 mg), and DMSO (3 mL) were mixed under hydrothermal assisted microwave for 20 min at 100 °C. The reaction mixture was allowed to cool, and the catalyst was separated from the reaction mixture by a magnetic bar. The filtrate was ran for a further 20 min, cooled, and analyzed with UV-Vis spectrophotometer.

## 4. Catalysts Characterization

Nitrogen sorption isotherms were obtained from using a Micromeritics (ASAP 2020) surface area analyzer at 77 K. Powder X-ray diffraction patterns of materials were recorded with X'Pert Pro X-ray diffractometer operated at a voltage of 45 Kv and current of 40 Ma. FTIR spectra of materials were recorded using Spotlight 400 spectrometer. Scanning electron microscopic images of the materials were obtained using JSM-7500F (JEOL, Tokyo, Japan) scanning electron microscope. Thermogravimetric analysis (TGA) of the samples was carried out using a TA, Q500 thermal analyzer (TA Instrument, New Castle, USA).

## 5. Conclusions

In summary, magnetic solid acid catalysts were successfully synthesized as heterogeneous catalysts by a three-step method. The triphenylamine, sulfonated, and magnetic polymers possess nanofibers, nanorods, and flake-like morphologies with higher surface areas. The FeSPPTPA80 catalyst showed very high catalytic activity for fructose dehydration to HMF than other catalysts, due to the nanorods that formed after sulfonation of neat PPTPA which gave it enough catalytic centers. The FeSPPTPA80 nanocatalyst could be recycled and reused for four consecutive reaction cycles without apparent leaching during the reaction, signifying high stability and reusability of the nanocatalyst.

## References

1. Pace, V.; Hoyos, P.; Castoldi, L.; de Maria, P.D.; Alcantara, A.R. 2-Methyltetrahydrofuran (2-MeTHF): A Biomass-Derived Solvent with Broad Application in Organic Chemistry. *ChemSusChem* **2012**, *5*, 1369–1379. [CrossRef] [PubMed]
2. Lange, J.; Prince, R.; Ayoub, P.M.; Louis, J.; Petrus, L.; Clarke, L.; Gosselink, H. Valeric biofuels: A platform of cellulosic transportation fuels. *Angew. Chem. Int. Ed.* **2010**, *49*, 4479–4483. [CrossRef] [PubMed]
3. Alonso, D.M.; Wettstein, S.G.; Dumesic, J.A. Gamma-valerolactone, A sustainable platform molecule derived from lignocellulosic biomass. *Green Chem.* **2013**, *15*, 584–595. [CrossRef]
4. Van Putten, R.J.; Waal, J.C.V.D.; Jong, E.D.; Rasrendra, C.B.; Heeres, H.J.; Vries, J.G.D. Hydroxymethylfurfural, A Versalile Platform Chemical made from Renewable Resources. *Chem. Rev.* **2013**, *113*, 1499–1597. [CrossRef] [PubMed]

5.  Balakrishnan, M.; Sacia, E.R.; Bell, A.T. Etherification and reductive etherification of 5-(hyroxymethyl)furfural: 5-(alkoxymethyl)furfurals and 2,5-bis (alkoxymethyl) furans as potential bio-diesel candidates. *Green Chem.* **2012**, *14*, 1626–1634. [CrossRef]

6.  Cai, J.Y.; Ma, H.; Zhang, J.J.; Song, Q.; Du, Z.T.; Huang, Y.Z.; Xu, J. Gold Nanoclusters Confined in a Supercage of Y Zeolite for Aerobic Oxidation of HMF under Mild Conditions. *J. Chem. Eur. J.* **2013**, *19*, 14215–14223. [CrossRef] [PubMed]

7.  Romàn-Leshkov, Y.; Barrett, C.J.; Liu, Z.Y.; Dumesic, J.A. Production of dimethylfuran for liquid fuels from biomass-derived carbohydrates. *Nature* **2007**, *447*, 982–985. [CrossRef] [PubMed]

8.  Ordomskiy, V.; van der Schaaf, J.; Schouten, J.C.; Nijhuis, T.A. The effect of solvent addition on fructose dehydration to 5-Hydroxymethylfurfural in biphasic system over zeolites. *J. Catal.* **2012**, *287*, 68–75. [CrossRef]

9.  Weingarten, R.; Rodriguez-Beuerman, A.; Cao, F.; Luterbacher, J.S.; Alonso, D.M.; Dumesic, J.A.; Huber, G.W. Selective Conversion of Cellulose to Hydroxymethylfurfural in Polar Aprotic Solvents. *ChemCatChem* **2014**, *6*, 2229–2234. [CrossRef]

10. Srinivasu, P.; Venkanna, D.; Kantam, M.L.; Tang, J.; Bhargava, S.K.; Aldalbahi, A.; Wu, K.C.W.; Yamauchi, Y. Ordered Hexagonal Mesoporous Aluminosilicates and their Application in Ligand-Free Synthesis of Secondary Amines. *ChemCatChem* **2015**, *7*, 747–751. [CrossRef]

11. Jackson, D.H.K.; Wang, D.; Gallo, J.M.R.; Crisci, A.J.; Scott, S.L.; Dumesic, J.A.; Kuech, T.F. Amine Catalyzed Atomic Layer Deposition of (3-Mercaptopropyl) trimethoxysilane for the Production of Heterogeneous Sulfonic Acid Catalysts. *Chem. Mater.* **2013**, *25*, 3844–3851. [CrossRef]

12. Wang, H.; Kong, Q.; Wang, Y.; Deng, T.; Chen, C.; Hou, X.; Zhu, Y. Graphene Oxide Catalyzed Dehydration of Fructose into 5-Hyfroxymethylfurfural with Isopropanol as Cosolvent. *ChemCatChem* **2014**, *6*, 728–732. [CrossRef]

13. Qi, L.; Mui, Y.F.; Lo, S.W.; Lui, M.Y.; Akien, G.R.; Horvath, I.T. Catalytic Conversion of Fructose, Glucose, and Sucrose to 5-(Hydroxymethyl)furfural and Levulinic and Formic Acids in γ-Valerolactone as a Green Solvent. *ACS Catal.* **2014**, *4*, 1470–1477. [CrossRef]

14. Chheda, J.N.; Roman-Leshkov, Y.; Dumesic, J.A. Production of 5-hydroxymethylfurfural and furfural by dehydration of biomass-derived mono- and polysaccharides. *Green Chem.* **2007**, *9*, 342–350. [CrossRef]

15. Hansen, T.S.; Woodley, J.M.; Riisager, A. Efficient microwave-assisted synthesis of 5-hydroxymethylfurfural from concentrated aqueous fructose. *Carbohydr. Res.* **2009**, *344*, 2568–2572. [CrossRef] [PubMed]

16. Salak Asghari, F.; Yoshida, H. Acid-Catalyzed Production of 5-Hydroxymethyl Furfural from D-Fructose in Subcritical Water. *Ind. Eng. Chem. Res.* **2006**, *45*, 2163–2173. [CrossRef]

17. Siankevich, S.; Fei, Z.; Scopelliti, R.; Laurenczy, G.; Katsyuba, S.; Yan, N.; Dyson, P.J. Enhanced conversion of carbohydrates to the platform chemical 5-hydroxymethylfurfural using designer ionic liquids. *ChemSusChem* **2014**, *7*, 1647–1654. [CrossRef]

18. Liu, J.; Yee, K.K.; Lo, K.K.W.; Zhang, K.Y.; To, W.P.; Che, C.M.; Xu, Z.T. Selective Ag(I) Binding, H2S Sensing, and White-Light Emmision from an Easy-to-Make Porous Conjugated Polymer. *J. Am. Chem. Soc.* **2014**, *136*, 2818–2824. [CrossRef]

19. Yang, F.L.; Liu, Q.; Yue, M.; Bai, X.; Du, Y. Tantalum compounds as heterogeneous catalysts for saccharide dehydration to 5-hydroxymethylfurfural. *Chem. Commun.* **2011**, *47*, 4469–4471. [CrossRef]

20. Nikolla, E.; Romàn-Leshkov, Y.; Moliner, M.; Davis, M.E. One-Pot Synthesis of 5-(Hydroxymethyl)furfural from Carbohydrates using Tin-Beta Zeolite. *ACS Catal.* **2011**, *1*, 408–410. [CrossRef]

21. Tong, X.; Ma, Y.; Li, Y. Biomass into chemicals: Conversion of sugars to furan derivatives by catalytic processes. *Appl. Catal. Gen.* **2010**, *385*, 1–13. [CrossRef]

22. Ling, P.; Hao, Q.; Lei, J.; Ju, H. Porphyrin fumctionalized porous carbon derived from metal-organic framework as a biomimetic catalyst for electrochemical biosensing. *J. Mater. Chem.* **2015**, *3*, 1335–1341. [CrossRef]

23. Pramanik, M.; Nandi, M.; Uyama, H.; Bhaumik, A. Organic-inorganic hydrid porous sulfonated zinc phosphonate material: Efficient catalysts for biodiesel synthesis at room temperature. *Green Chem.* **2012**, *14*, 2273–2281. [CrossRef]

24. Mondal, S.; Mondal, J.; Bhaumik, A. Sulfonated Porous Polymeric Nanofibers as an Efficient Solid Acid Catalyst for the Production of 5-Hydroxymethylfurfural from Biomass. *ChemCatChem* **2015**, *7*, 3570–3578. [CrossRef]

25. Amarasekara, A.S.; Williams, L.D.; Ebede, C.C. Mechanism of the dehydration of D-fructose to 5-hydroxymethylfurfural in dimethyl sulfoxide at 150 degrees C: An NMR study. *Carbohydr. Res.* **2008**, *343*, 3021–3024. [CrossRef] [PubMed]

26. Caratzoulas, S.; Vlachos, D.G. Converting fructose to 5-hydroxymethylfurfural: A quantum mechanics/molecular mechanics study of the mechanism and energetics. *Carbohydr. Res.* **2011**, *346*, 664–672. [CrossRef] [PubMed]

27. Zhu, H.; Cao, Q.; Li, C.; Mu, X. Acidic resin-catalysed conversion of fructose into furan derivatives in low boiling point solvents. *Carbohydr. Res.* **2011**, *346*, 2016–2018. [CrossRef]

28. Yang, Y.; Du, Z.; Ma, J.; Lu, F.; Zhang, J.; Xu, J. Biphasic catalytic conversion of fructose by continuous hydrogenation of HMF over a hydrophobic ruthenium catalyst. *ChemSusChem* **2014**, *7*, 1352–1356. [CrossRef]

29. Ma, M.; Zhang, Y.; Yu, W.; Shen, H.; Zhang, H.; Gu, N. Preparation and Characterization of Magnetite Nanoparticles Coated by Amino Silane. *Colloids Surf. Physicochem. Eng. Asp.* **2003**, *212*, 219–226. [CrossRef]